JOURNAL OF MATERIALS SCIENCE **34** (1999) 4793–4802

X-ray diffraction characterisation of low temperature plasma nitrided austenitic stainless steels

Y. SUN*, X. Y. LI, T. BELL
School of Metallurgy and Materials, University of Birmingham, Birmingham B15 2TT, UK
E-mail: suny@novell2.bham.ac.uk

The nitrided layers produced by low temperature (400–500 °C) plasma nitriding on austenitic stainless steels, AISI 316, 304 and 321, have been characterised by X-ray diffraction, in conjunction with metallographic and chemical composition profile analysis. The thin, hard and corrosion resistant layers exhibited similar X-ray diffraction patterns, but the positions of the major diffraction peaks varied with nitriding temperature and nitrogen concentration profile. The low temperature nitrided layers are predominantly composed of a phase with a face centred cubic (fcc) structure, which is named "S" phase. However, the positions of the diffraction peaks from the "S" phase deviated in a systematic way from those for an ideal fcc lattice. Detailed analysis of the deviation suggested that very high compressive residual stresses and stacking faults were formed in the layers, resulting in a highly distorted and disordered fcc structure. The lattice parameter of the distorted and disordered "S" phase was found to increase with increasing nitrogen concentration.

1. Introduction

Nitriding has been used for many years to engineer the surfaces of austenitic stainless steels to improve their surface hardness and tribological properties [1, 2]. Nitriding of austenitic stainless steels is usually characterised by the precipitation of chromium nitrides in the nitrided case, inducing precipitation hardening. This leads to a depletion of the chromium content in the austenitic matrix, and thus a significant reduction in the corrosion resistance of the nitrided layer [3].

Attempts have accordingly been made in the past decade to improve the corrosion resistance of nitrided austenitic stainless steels. One of these attempts involved plasma nitriding at relatively low temperatures, normally lower than 450 °C [4], rather than at conventional nitriding temperatures of around 600 °C used for austenitic stainless steels. It has been found by many investigators that at low temperatures, plasma nitriding can produce a thin layer of extremely high hardness with excellent corrosion resistance [5, 6]. This phenomenon has also been observed in gas nitriding [7] and more recently in plasma immersion ion implantation (PIII) of austenitic stainless steels at temperatures between 350 and 450 °C [8].

The low temperature nitrided layers produced on austenitic stainless steels were considered to be precipitation-free and composed of an uncharacterised phase. This was regarded as an expanded austenite by some investigators [7, 9], and resulted from the supersaturation of nitrogen in austenite. X-ray diffraction of the nitrided surfaces normally produced some broad peaks at diffraction angles lower than the substrate austenite peaks. The uncharacterised phase in the nitrided layer was also referred to as 'S' phase by several investigators [5, 6, 9, 10] since it was not identified according to the ASTM X-ray Diffraction Index. This phase was also regarded as a metastable supersaturated solid solution with a disordered face centred cubic (fcc) structure [11]. On the other hand, some investigators suggested that the X-ray diffraction peaks from low temperature nitrided surfaces corresponded to a phase with a body-centred tetragonal (bct) structure [8]. Transmission electron microscopy (TEM) has recently been employed to characterise structures in PIII treated austenitic stainless steel [12]. TEM studies revealed a complicated structure in the treated layer, but could not satisfactorily explain the X-ray diffraction results.

Clearly, the structures of the hard and corrosion resistant layers produced by nitriding at low temperatures are far from being fully understood, and the nature of the "S" phase has not been fully characterised. Most of the results obtained and conclusions made so far have been based on limited experimental work. The purpose of the present work was therefore to characterise the structures (particularly the "S" phase") of low temperature plasma nitrided layers by carrying out a series of plasma nitriding experiments at various temperatures

* Author to whom all correspondence should be addressed.

on three different austenitic stainless steels, and then performing detailed X-ray diffraction analysis and metallographic examination of the nitrided surfaces.

2. Experimental Details

Three austenitic stainless steels have been investigated in the present work, namely AISI 316, 304 and 321 steels. The chemical compositions of these steels are shown in Table I. Plasma nitriding specimens 24.5 mm in diameter and 8 mm in thickness were machined from 25.4 mm diameter hot rolled bars. The specimens were then manually ground using SiC grinding papers down to 1200 grade to achieve a fine finish.

The original structures of the steels comprised of equiaxed grains of austenite with some growing twins, without any ferrite detectable by X-ray and metallography. However, at the circumference of each of the as-received hot rolled bars, there was evidence of a heavily deformed layer of about 0.3 mm thick. Most of the nitriding specimens were prepared by machining to remove the deformed layer. But some specimens were prepared without removing the deformed layer, so that the effect of prior deformation on nitriding response could also be investigated.

Plasma nitriding was carried out using a 60 kW Klochner DC plasma nitriding unit. In the present work, the austenitic stainless steel specimens were nitrided at various temperatures between 400 and 600 °C. All of the nitriding experiments were performed in a 25% N_2 + 75% H_2 treatment atmosphere, at a pressure of 5 mbar and for a similar time of 5 h.

X-ray diffraction analysis of nitrided surfaces was performed using a Philips X-ray diffractometer with CoK_α and CuK_α radiations. A 2θ angle range of 30° to 140° was selected with a scanning speed of 0.5°/min. Since the nitrided layers were generally thin (less than 20 μm), most of the X-ray analysis was performed directly on the as-nitrided surface. But in order to obtain more information, selected samples were polished or slightly ground to remove successive layers before X-ray diffraction analysis.

TABLE I Chemical compositions of the investigated austenitic stainless steels (wt %)

AISI	Cr	Ni	Mo	Ti	Mn	C
316	19.23	11.26	2.67	0.00	1.86	0.06
304	18.45	10.54	0.00	0.00	2.00	0.07
321	18.78	11.04	0.00	0.28	1.91	0.06

Standard procedures were followed to prepare metallographic specimens of the cross sections of the nitrided samples. This involved nickel-plating for nitrided layer protection, mounting, grinding and polishing. The polished specimens were then etched in a solution containing 50 vol % HCl + 25 vol % HNO_3 + 25 vol % H_2O. In order to reveal more microstructural features, oblique sections of selected nitrided specimens were prepared at an inclined angle of 5° to the nitrided surface and then etched electrolytically in saturated aqueous oxalic solution.

Nitrogen concentration profiles through nitrided layers were analysed using a Leco GDS-750 glow discharge spectrometer. Details of the technique have been reported elsewhere [13]. A γ'-Fe_4N layer produced by plasma nitriding on Armco iron was used to calibrate the nitrogen concentration. While this calibration technique provides reasonable accuracy for nitrided low alloy steels, its applicability to such high alloy steels as stainless steels is not fully justified. However, glow discharge spectrometry (GDS) can at least provide semi-quantitative information on the distribution of nitrogen in the nitrided layers concerned in the present work.

3. Results

3.1. Morphology of nitrided layers

Plasma nitriding of the austenitic stainless steels at temperatures between 400 and 600 °C produced three different metallographic structures, as illustrated in Fig. 1 for 316 steel. It is clearly seen that at low temperatures a thin "white" layer was produced on the steel surface. The thickness of the 'white' layer ranged from several micrometers to 20 micrometers, depending on processing temperature and time. The whitish appearance of the nitrided layer may indicate good corrosion resistance of the layer in the etchants used. Corrosion testing in other solutions also demonstrated the corrosion resistant nature of the low temperature nitrided layers [1, 6, 9]. With increasing temperature, some dark phases began to form in the "white" layer, resulting in

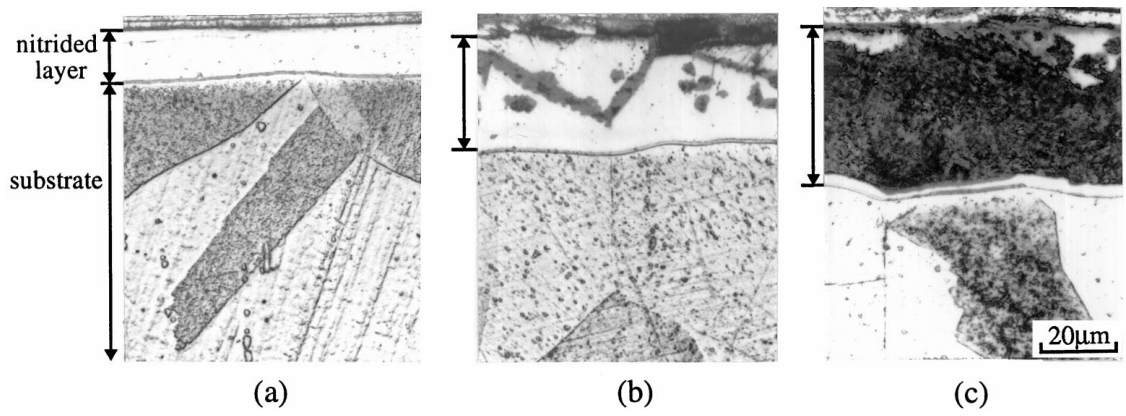

Figure 1 Optical micrographs of microsections of AISI 316 steel nitrided at (a) 450 °C; (b) 500 °C and (c) 525 °C for 5 h.

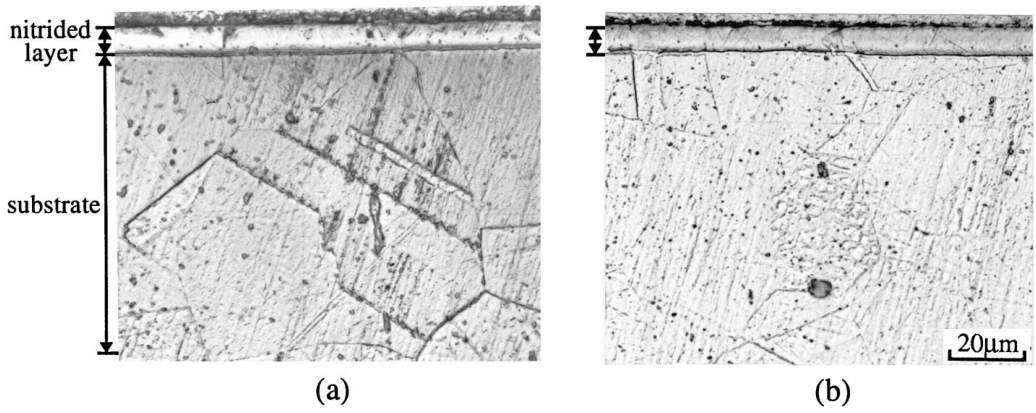

Figure 2 Optical micrographs of microsections of (a) 304 steel and (b) 321 steel nitrided at 425 °C for 5 h.

a nitrided layer of mixed "white" and "black" phases. At temperatures of 525 °C and above, the nitrided layer is completely "black", this being typical of conventional nitriding of austenitic stainless steels [4]. All three types of austenitic stainless steels investigated in the present work revealed metallographic structures similar to those shown in Fig. 1. But the transition temperatures from a "white" layer to a mixed "white" and "black" layer and then to a completely "black" layer vary slightly for different steels. The reasons behind this will be discussed elsewhere. Fig. 2 shows the optical micrographs of the cross sections of 304 and 321 steel nitrided at 425 °C. It is clear that a "white" layer can also form on these two steel surfaces.

Since the nitrided layers produced at low temperatures are usually very thin (less than 15 μm), their detailed structures can hardly be revealed in the cross sections. Accordingly, tapered sections at an inclined angle 5° to the surface were prepared. Typical structures of the layer produced at 450 °C on 316 steel are shown in Fig. 3. Several microstructural features were observed in the oblique sections. The nitrided layer seemed to have reproduced the morphological features existent in the substrate, evidenced by the continuation of substrate austenite grains and twins in the nitrided layer, some of which even continue from the substrate through the nitrided layer to the surface (Fig. 3a). The reproduction of substrate morphological features in the layer is even more evident when the edges of the specimen were examined, where a prior deformed layer existed (Fig. 3b). The original slip lines and deformation bands were precisely reproduced in the nitrided layer, some of which linked the substrate and the layer together. However, the slip lines in the nitrided layer in the prior deformed areas became curved, indicating a high degree of lattice distortion in the layer (Fig. 3b). In the central area of the specimen, no slip lines were observed in the substrate, but some short and straight slip lines were evident in the nitrided layer (Fig. 3c), probably induced during the growth of the layer.

Other structural features observed in the oblique sections include a thin and heavily etched film on the surface and grain boundary precipitation evidenced by the heavily etching of the original austenite grain boundaries in the near surface region. The thin surface film (less than 0.5 μm) has a columnar morphology and is identified as comprising mainly $\gamma' - (Fe,Cr)_4N$ phase as discussed later.

3.2. X-ray diffraction patterns

A detailed microstructural analysis of the nitrided layers produced over the whole temperature range, particularly at relatively high temperatures is beyond the scope of this paper, which will concentrate on the X-ray diffraction characteristics of low temperature nitrided surfaces with predominantly a "white" layer. X-ray diffraction patterns from the 316 steel samples nitrided at 400 to 500 °C are shown in Fig. 4. Although the X-ray diffraction analysis was performed for 2θ angles ranging between 30° and 140°, only the diffraction peaks produced between 40° and 65° are shown in Fig. 4 for clarity. For easy analysis, diffraction angle positions for various possible phases in the nitrided chromium bearing stainless steels are also shown in Fig. 4, i.e. austenite (γ), ferrite (α), chromium nitrides (CrN and Cr_2N), and iron nitrides (γ'-Fe_4N and ε-$Fe_{2\text{-}3}N$).

From Fig. 4 the variation of the X-ray diffraction patterns with nitriding temperature can be clearly seen. At 400 °C, a very thin nitrided layer was produced (2–3 μm) and thus two strong peaks from the substrate were obtained, corresponding to fcc $\gamma(111)$ and $\gamma(200)$ planes. Two broad peaks, designated S1 and S2, were also present from the nitrided layer. Both the S1 and S2 peaks occurred at a lower 2θ angle than the $\gamma(111)$ and $\gamma(200)$ peaks respectively. The S2 peak seems to be associated with $\gamma'(200)$ for the 400 °C nitrided sample. However, for reasons described below, S1 and S2 were from the same structure and S2 was not the result of the diffraction of the $\gamma'(200)$ plane. At 425 °C, a similar diffraction pattern was produced, but the diffraction intensity of $\gamma(111)$ and $\gamma(200)$ peaks were reduced and that of S1 and S2 was increased, due to a thicker nitrided layer (7–8 μm) produced at this temperature. In addition, the S1 and S2 peaks shifted concurrently to lower 2θ angles. At 450 °C, the nitrided layer is sufficiently thick (12 μm) such that only weak diffraction peaks were produced from the fcc substrate. A new peak, corresponding to γ' (200) was obtained. The $\gamma'(200)$ peak was observed in the diffraction patterns of all of the samples nitrided at 450 °C and above. At 450 °C, the

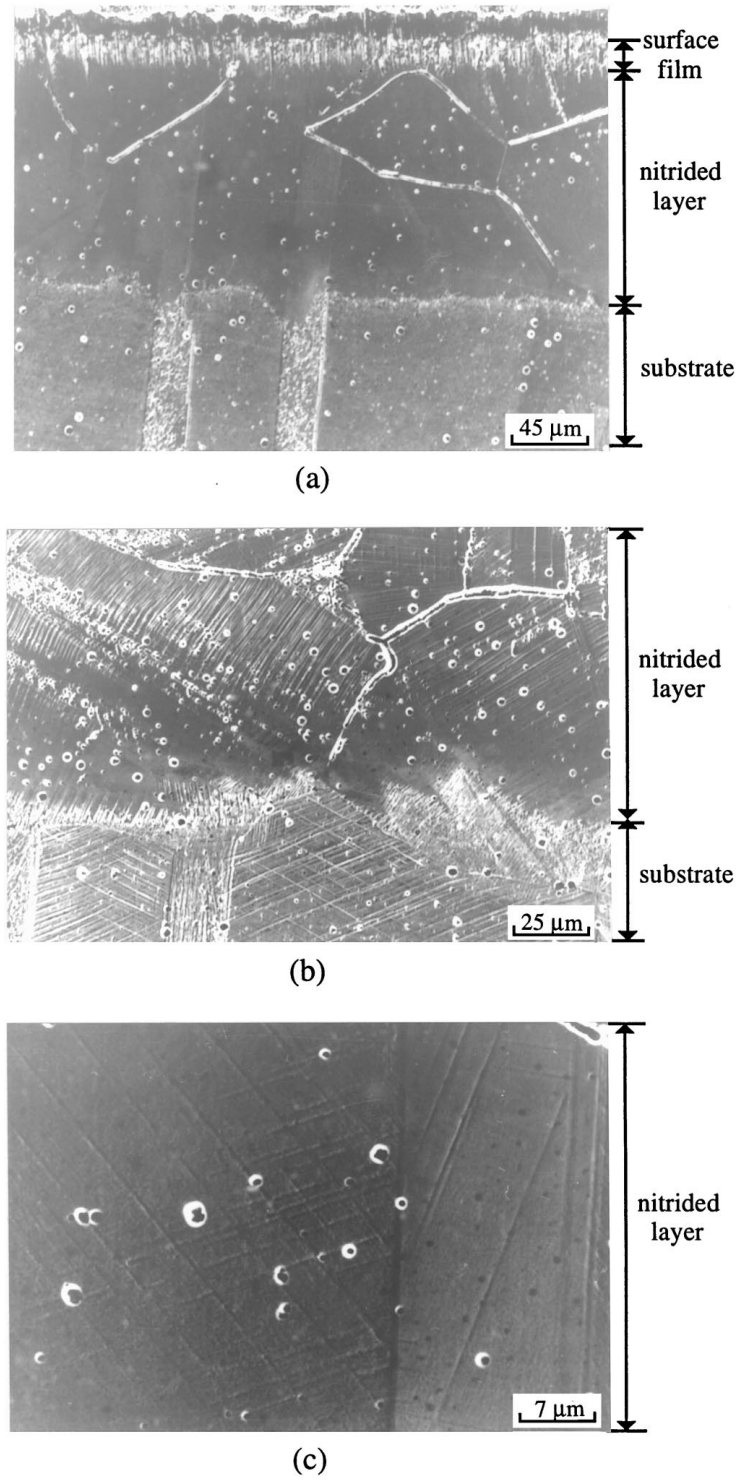

Figure 3 Scanning electron micrographs of the taper section at an inclined angle 5° to the surface of 316 steel nitrided at 450 °C for 5 h: (a) central area; (b) edge area and (c) slip lines in central area.

S1 and S2 peaks further shifted to lower angles. This shift continued, although to a lesser extent, at 475 and 500 °C. But at 500 °C, the intensity of the S2 peak became much lower such that it was hardly able to be identified. This is due to the precipitation of CrN in the nitrided layer, resulting in a mixed "white" and "black" layer (Fig. 1).

Similar X-ray diffraction patterns were also obtained for the low temperature nitrided 304 and 321 steels. Fig. 5 shows the X-ray diffraction patterns of 304 and 321 samples nitrided at 425 °C. The variation of the diffraction patterns with nitriding temperature in 304 and 321 steel was also similar to that in 316 steel described above.

The variation of X-ray diffraction patterns with depth from the nitrided surface is illustrated in Fig. 6, which shows that as the nitrided layer was gradually removed, the S1 and S2 peaks shifted to higher 2θ angles, gradually towards the positions for the fcc γ (111) and γ(200) peaks respectively.

From the variation of the X-ray diffraction patterns with nitriding temperature, it is clear that the positions of the S1 and S2 peaks moved concurrently to lower angles with increasing nitriding temperature from 400

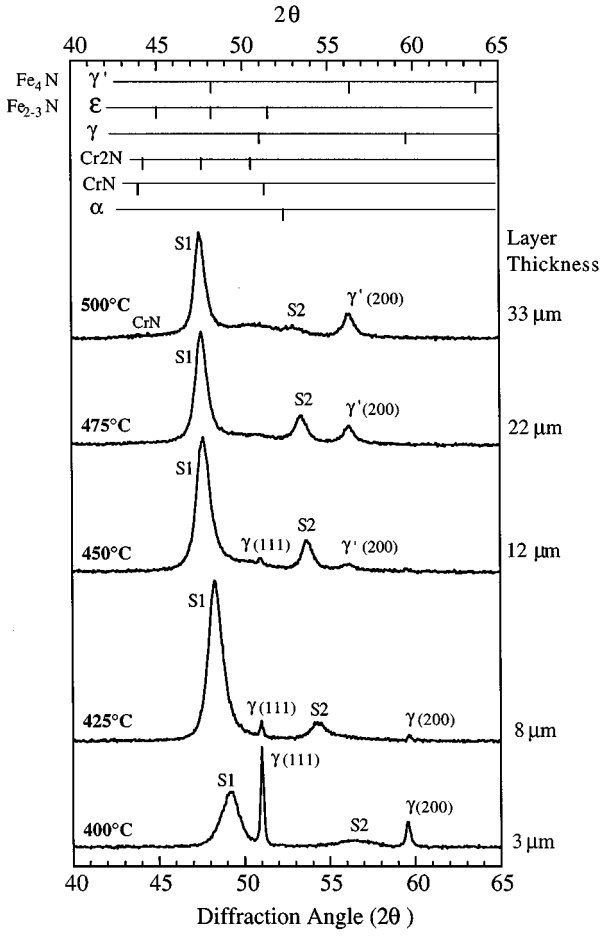

Figure 4 X-ray diffraction patterns (Co radiation) of AISI 316 steel nitrided at various temperatures.

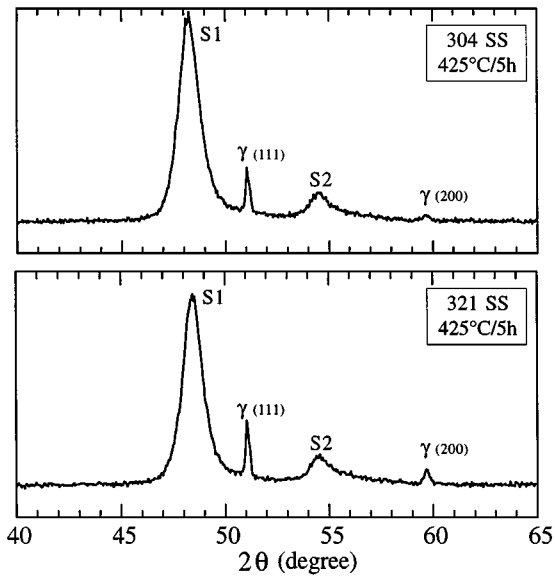

Figure 5 X-ray diffraction patterns (Co radiation) from 304 and 321 steel nitrided at 425 °C for 5 h.

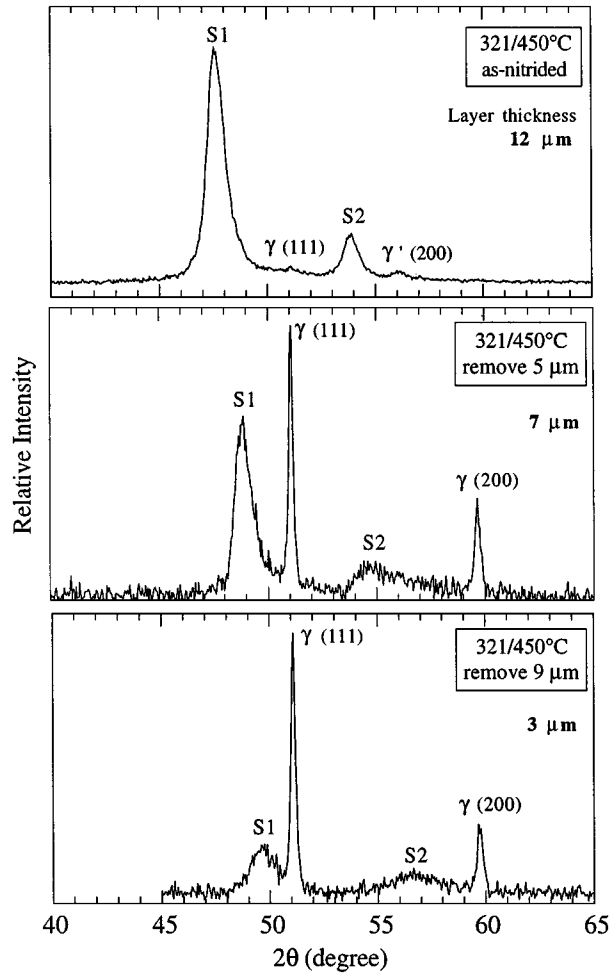

Figure 6 X-ray diffraction patterns (Co radiation) of AISI 321 steel, after successive layers of 0.0, 5 and 9 μm thick were removed from the nitrided layer of 12 μm thick.

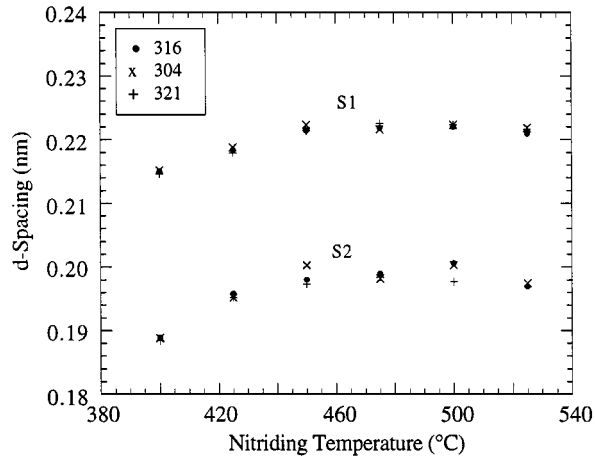

Figure 7 Variation of d_{S1} and d_{S2} with nitriding temperature.

to 500 °C. The interplanar spacings (i.e. *d*-spacings) corresponding to the S1 and S2 peaks, d_{S1} and d_{S2} respectively, for the three investigated steels are plotted in Fig. 7 vs. nitriding temperature, from which it can be seen that the three steels exhibited similar d_{S1} and d_{S2} values at the same temperatures and similar variation of the *d*-spacing values with temperature. From Fig. 7 it is also clear that the variation of d_{S1} with temperature is similar to that of d_{S2} with temperature, indicating that both S1 and S2 are the result of the same structure. The continuous variation of d_{S1} and d_{S2} with temperature also indicates that the nitrided layers produced at temperatures between 400 and 500 °C are predominantly composed of a single phase, which has the same crystal structure but varied lattice parameter(s) at different temperatures.

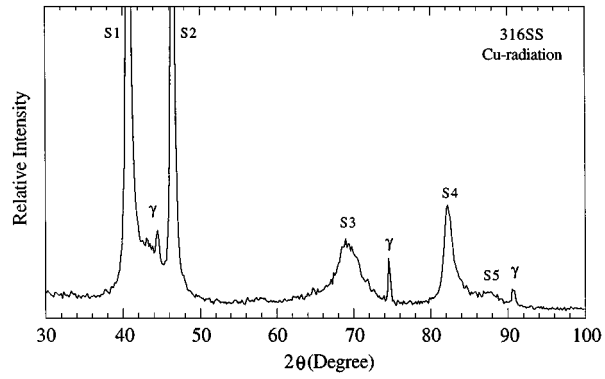

Figure 8 X-ray diffraction pattern (Cu radiation) from low temperature nitrided AISI 316 steel, sowing the high angle reflections.

In order to characterise the S1 and S2 peaks and thus the dominant phase in the nitrided layer, X-ray diffraction patterns at higher 2θ angles were examined. A typical pattern resulted from Cu$K_{\alpha 1}$ radiation covering 2θ angles in the range 30°–100° is shown in Fig. 8. Several broad peaks of low intensity are evident at high reflection angles, which do not correspond to any known phases in nitrided stainless steels. The positions of these peaks also shifted with nitriding temperature in a manner similar to that for the S1 and S2 peaks. These peaks were thus respectively designated S3, S4 and S5.

3.3. Nitrogen concentration profiles

Typical nitrogen concentration profiles as measured by GDS through the nitrided layers are given in Fig. 9 for 304 and 316 steel. From Fig. 9, the development of the nitrided layer and the associated nitrogen profile with temperature can be clearly seen. With increasing temperature from 400 to 475 °C, the nitrogen concentration in the nitrided layer increased. A very steep nitrogen profile was obtained in the 400 °C treated sample. With increasing temperature, a nitrogen plateau was gradually built-up, such that a similar level of nitrogen plateau was produced at 475 and 500 °C.

In all the samples analysed, very high nitrogen concentrations were obtained in the near surface region, which may be resulted from surface contamination and pore formation in the outer part of the layer, which is characteristic of plasma processing involving sputtering [13]. The high nitrogen concentration in the outer part of the layer may also indicate excess nitrogen uptake due to the formation of defects such as dislocations, pores and stacking faults, and the precipitation of nitrides at these defects and grain boundaries (see Fig. 3). Excess nitrogen uptake has been frequently observed in nitriding of low alloy ferritic steels [14].

4. Discussion

From Figs 4 and 6 it is clear that interpretation of the nitrided structure according to an individual X-ray diffraction pattern maybe misleading. Although at certain temperatures, the S1 or the S2 peak appeared at the position close to that for the γ' phase, the possibility that the S1 and S2 peaks would correspond to γ' (111)

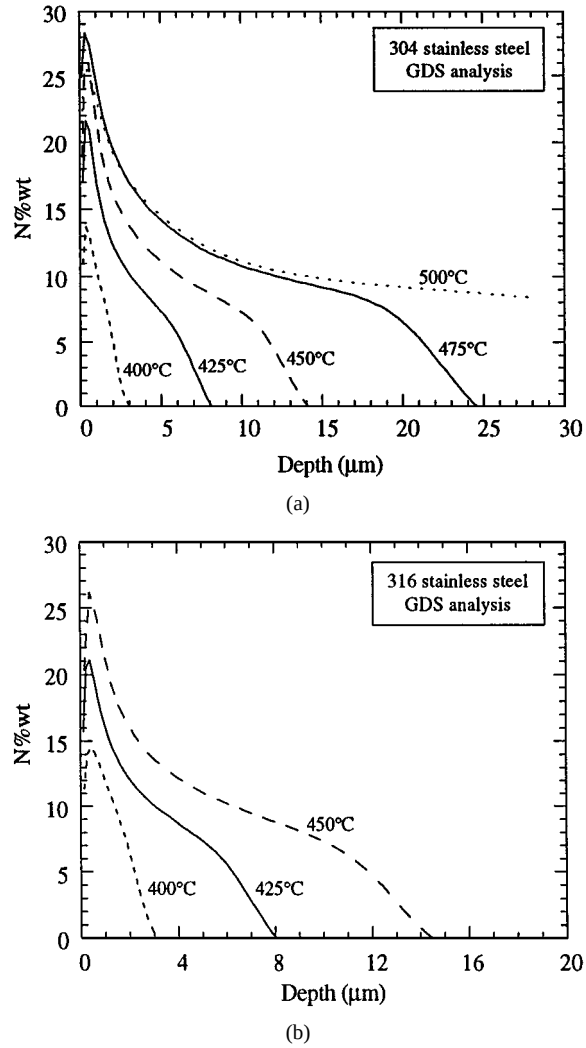

Figure 9 Typical nitrogen concentration profiles measured by GDS in (a) AISI 304 and (b) 316 steels nitrided at various temperatures.

and γ' (200) respectively can be ruled out, not only because the positions of S1 and S2 varied with temperature, but also because a separate diffraction peak corresponding to γ' (200) was obtained at 450 °C and above, the position of which did not vary with temperature. There is evidence to suggest that the γ' phase was formed on the major nitrided layer as a thin film of 0.1–0.5 μm thick with strong (200) orientation (Fig. 3). This explains the absence of the (111) peak for γ' in the X-ray diffraction patterns.

The possibility of overlapping of several peaks of various phases to produce the observed broad peaks can also be ruled out, since overlapping of several phases may result in a broad peak, but it is impossible to simultaneously produce several broad peaks such as S1 and S2, unless these phases have similar crystal structure and lattice parameters. Indeed, from Fig. 4 it can be seen that all the known phases which are possible in nitrided austenitic stainless steels can not produce strong overlap peaks at the S1 and S2 positions. Clearly, the S peaks, although very broad, are the diffraction peaks predominantly from a single phase, which is a dominant phase in the low temperature nitrided layers.

The predominant phase (i.e. “S” phase) in the low temperature nitrided layer was usually considered to

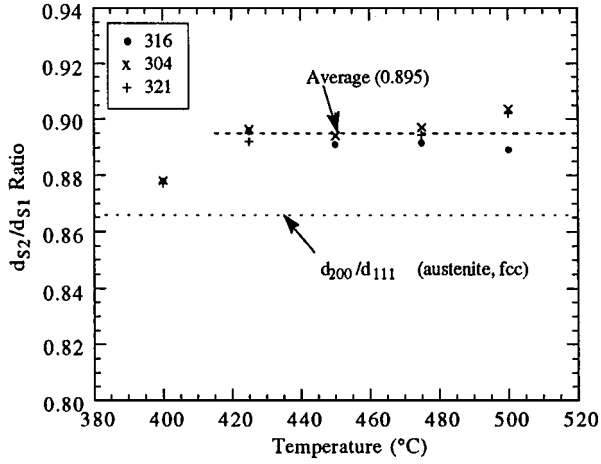

Figure 10 Variation of the ratio of d_{S2} to d_{S1} with nitriding temperature for AISI 316, 304 and 321 steels.

have an fcc structure and S1 and S2 correspond to (111) and (200) planes respectively [7, 9, 10]. However, a closer examination of the diffraction patterns shown in Fig. 4 and the d-spacings shown in Fig. 7 revealed that the ratio of d_{S2} to d_{S1} significantly deviates from that of d_{200} to d_{111} for an ideal fcc lattice. Fig. 10 shows the plot of the ratio of d_{S2} to d_{S1} as a function of nitriding temperature for the three investigated materials. For an ideal fcc structure, $d_{200}/d_{111} = 0.866$. Only at the nitriding temperature of 400 °C is the ratio of d_{S2} to d_{S1} (0.878) close to that for an ideal fcc structure. At higher temperatures, the d_{S2}/d_{S1} ratio increases to 0.895 (average). This discrepancy is obviously too large to be accounted for by experimental and instrumental errors.

It thus seems that the 'S' phase may have a body-centred tetragonal (bct) structure, as proposed by Samandi *et al.* [8]. In this case, S1 and S2 would correspond to (101) and (002) planes respectively, then a rough estimation of the lattice parameters a and c, could be easily made (e.g. $a = 0.267$, $c = 0.396$ at 450 °C for 316 steel). With such a large c/a ratio, more diffraction peaks would be expected in the 2θ angle range used in the present work. However, no diffraction peaks corresponding to the bct structure with a c/a ratio around 1.5 were detected.

If a fcc structure is assumed for the "S" phase, then S1, S2, S3, S4 and S5 should correspond to S(111), S(200), S(220), S(311) and S(222) respectively, and the lattice parameter, a_{hkl}, can then be estimated from each peak. For an ideal fcc structure, a plot of a_{hkl} vs. $\cos\theta\cot\theta$ gives a straight line which intersects with the vertical axis to give the true lattice parameter (a_0). Fig. 11 shows such plots for the untreated and the 450 °C treated 316 samples. All the points from the untreated sample fall neatly on a straight line intersecting with the vertical axis at 0.3596 nm. On the other hand, the data points for the nitrided sample show a large scatter, such that a straight line cannot be made to pass through all the points. However, a closer examination of Fig. 11 reveals that the scatter of the data points for the nitrided samples occur in a systematic way similar to that observed in X-ray diffraction of highly stressed and/or plastically deformed austenitic

TABLE II Fault parameter and elastic constant values for various reflections

hkl	$G_{hkl} \times 10^2$	$(S_1)_{hkl} \times 10^5$ (kg/mm^2)
111	−3.45	−0.97
200	+6.89	−2.97
220	−3.45	−1.47
311	+1.25	−2.03
222	+1.73	−0.97
400	−3.45	−2.97

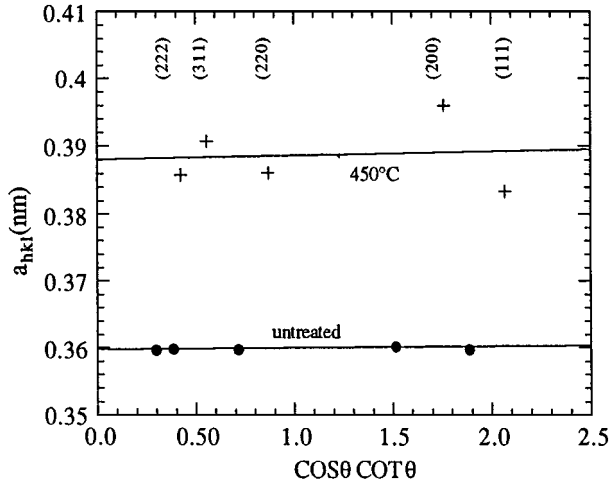

Figure 11 Plots of a_{hkl} vs. $\cos\theta\cot\theta$ for untreated and 450 °C nitrided 316 steel.

stainless steels [15, 16] and other fcc metals [17, 18]. It has been well established that stacking faults in fcc lattices (e.g. induced by plastic deformation) can influence not only the profiles (peak broadening) but also the positions (peak shift) of the X-ray diffraction peaks [19]. Similarly, residual stresses in the material can also result in a peak shift, the degree of which depends on the stress level (σ) and the elastic constant of the diffracting plane [17].

According to the theories of Paterson [19] and Warren [20], if stacking faults with a probability α are present in the material, then a change in lattice parameter Δa_{hkl}, which depends on the indices of reflection (hkl), is related to stacking fault probability by the following equation [17]:

$$\Delta a_{hkl} = a_0 G_{hkl} \alpha \tag{1}$$

where G_{hkl} is the stacking fault parameter, values for which are given in Table II for various reflections. It can be seen that as a result of stacking faults, the (200) peak is shifted to a lower angle whilst the (111) peak shifted to a higher angle, such that a higher d_{200}/d_{111} ratio is resulted.

On the other hand, if residual stresses are present in the material, then the change in lattice parameter is given by [17]

$$\Delta a_{hkl} = a_0 (S_1)_{hkl} \sigma \tag{2}$$

where $(S_1)_{hkl}$ is the elastic constant and σ is the residual stress. Since the crystal structure and elastic properties

of the "S" phase are unknown, it is impossible to estimate the $(S_1)_{hkl}$ values for the "S" phase. However, $(S_1)_{hkl}$ values for an austenitic Fe-Cr-Ni alloy are listed in Table II [21], from which it can be seen that compressive residual stresses in fcc austenite cause all the diffraction peaks to shift to lower angles (i.e. lattice expansion). But the degree of peak shift is three times larger for the (200) plane than for the (111) plane due to the higher elastic constant in the [200] direction than in the [111] direction. This also results in a higher d_{200}/d_{111} ratio.

Clearly, the combined effect of stacking faults and compressive residual stresses will result in a further increase in the d_{200}/d_{111} ratio. Fig. 12 shows the plots of $\Delta a_{hkl}/a_0$ vs. $\cos\theta\cot\theta$ assuming (a) $\alpha = 0.1$, $\sigma = 0$; (b) $\alpha = 0$, $\sigma = 100$ kg/mm^2; and (c) $\alpha = 0.1$, $\sigma =$ 100 kg/mm^2, for fcc austenite, illustrating the effect of stacking faults and residual stresses, as well as the combination of these two factors on data scattering with respect to the correct straight lines which were drawn following the approach of Wagner *et al.* [17]. It can be seen that stacking faults and compressive stresses cause similar data scatter, except for the data point for the second order reflections (e.g. (222)). For example, the (222) point lies above the correct line when stacking fault effect is dominant, but lies below the correct line when stress effect is dominated. It is the difference in the second order reflections that enables the difference between stacking fault and residual stress effects to be distinguished.

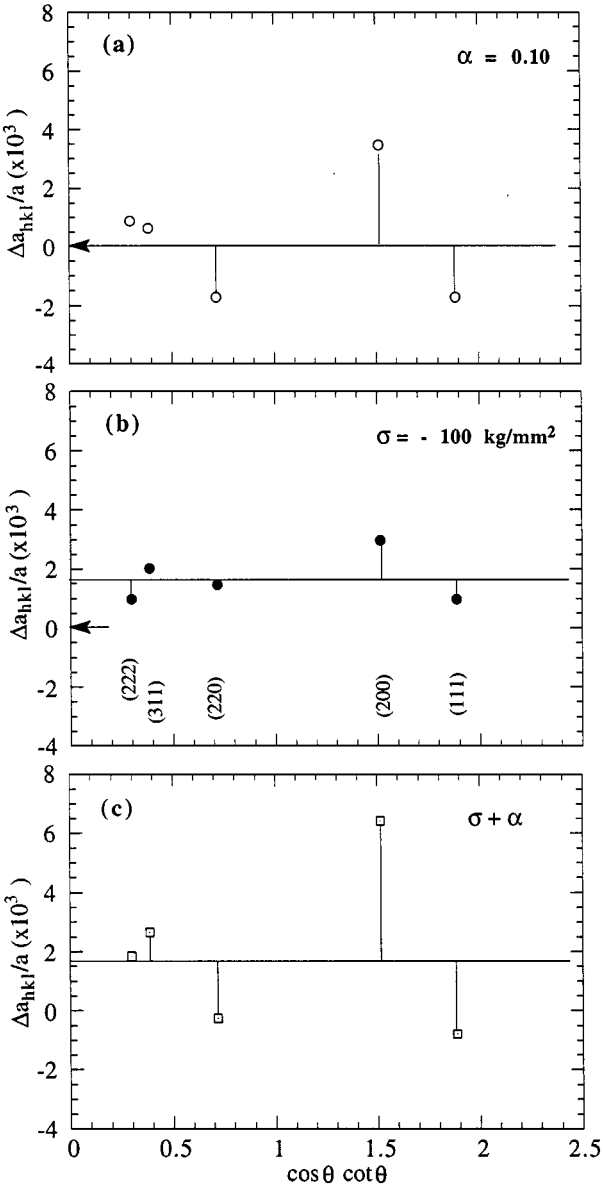

Figure 12 Plots of $\Delta a_{hkl}/a_0$ vs. $\cos\theta\cot\theta$ for Fe-Cr-Ni austenitic alloy assuming (a) $\alpha = 0.1$; (b) $\sigma = 100$ kg/mm^2 and (c) $\alpha = 0.1$, $\sigma = 100$ kg/mm^2.

Without knowing the lattice parameter of the stress-free and fault-free "S" phase in the nitrided layer, it is not possible to accurately evaluate the relative contribution of stacking faults and residual stresses to the observed peak shifts. However, a comparison of Fig. 11 with Fig. 12 demonstrated that compressive residual stresses have a strong effect on the peak shift of the investigated "S" phase. There is sufficient evidence to suggest that very high residual stresses were induced in the nitrided layers produced at low temperatures. The observed curvature of the prior existing slip lines is a good indication of high stresses and lattice distortion (Fig. 3b). In fact, the internal stress was so high that cracks were frequently observed in the nitrided layer under the optical microscope, such that the low temperature nitrided layers were regarded as being very brittle [6]. In order to further evaluate the effect of residual stress on X-ray diffraction peak shift, nitriding experiments have been carried out using thin foil specimens of 50 μm thick. The stress level in the nitrided layer is expected to be much lower in thin foil specimens than in thick specimens, since there is less substrate material in the foil to accommodate the stress in the surface layer and stress relaxation is thus expected in the nitrided layer. The X-ray diffraction results for the thin foil specimen nitrided to produce a layer of 10 μm on both faces of the foil are illustrated in Fig. 13, together with those from the thick specimen with similar layer thickness. It can be seen that the data points from the thick specimen are very scattered, and the (222) point lies below and the (400) point lies above the correct straight line, indicating the existence of very high compressive stresses. On the other hand, the data points

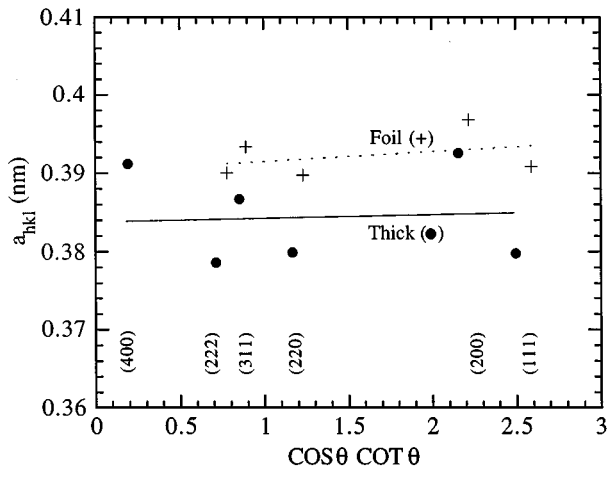

Figure 13 Plots of a_{hkl} vs. $\cos\theta\cot\theta$ for low temperature nitrided AISI 316 thin foil and thick specimens.

from the thin foil specimen are much less scattered and the (222) point moves close to the straight line. These results indicate that the lattice of the 'S' phase formed in the thin foil specimen is closer to the idea fcc lattice, obviously due to the much reduced residual stress level.

Data scattering, although to a lesser extent, is still evident in thin foil specimens. The contribution of stacking faults should be taken into account. Although metallographic examination of the nitrided surface structure could not directly reveal the presence of stacking faults in the nitrided layer, it did reveal some slip lines induced by the growth of the nitrided layer (Fig. 3c). These slip lines were straight and different from the prior existing slip lines which were curved in the nitrided layer (Fig. 3b). The formation of slip lines/bands is a structural feature typical of deformed fcc metals and alloys, which is usually accompanied with the formation of stacking faults [18]. The formation of faults in the nitrided layer may be facilitated by the high internal stresses and strains induced in the layer, and the supersaturation of nitrogen which is known to reduce the stacking fault energy in austenitic stainless steels [22]. Recent TEM studies made by the present authors also indicate the formation of stacking faults in the nitrided layer [23]. The formation of stacking faults may also explain the thin platelets of a hexagonal phase observed by Hannula *et. al.* [24] in the 350 °C nitrided layer on 316 steel.

From the above analysis, it is concluded that the "S" phase produced by plasma nitriding of austenitic stainless steels, which is the main constituent in low temperature nitrided layers, has an fcc structure which is highly disordered and distorted, due to the formation of stacking faults and high compressive residual stresses in the nitrided layer.

Since stacking faults and compressive residual stresses cause the shift of the (111) peak in opposite directions, the lattice parameter of the "S" phase was estimated using the S1 peak in the present work. Fig. 14 shows the variation of a_{S1} with nitriding temperature and depth from the surface. It is evident that the lattice parameter increases with nitriding temperature and decreases with depth from the surface. With reference to the measured nitrogen concentration profiles (Fig. 9), it is clear that the lattice parameter of the "S" phase increases with nitrogen concentration, such that the lattice parameter and degree of lattice distortion of the "S" phase gradually decrease towards the layer-core interface. Clearly, the 'S' phase is gradually expanded and distorted from the interface towards the surface.

Although chromium nitride precipitation was only detected at temperatures 500 °C and above for 316 steel and at 450 °C and above for 304 and 321 steels, the measured nitrogen concentration profiles (Fig. 9) and the observed surface structure (Fig. 3) may indicate precipitation of nitrides at lower temperatures, which may be responsible for the excessively high surface nitrogen concentration. The X-ray diffraction technique employed has insufficient resolution to detect minor constituents in the nitrided layer. More detailed structural studies of low temperature plasma nitrided austenitic stainless steels are currently being carried out using transmission electron microscope [25].

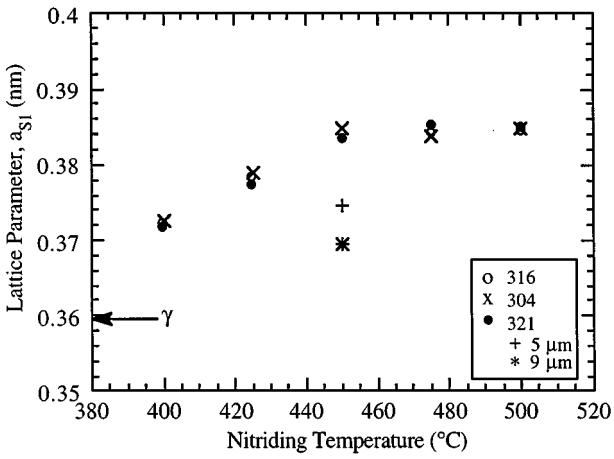

Figure 14 Variation of lattice parameter (a_{S1}) of the 'S' phase with nitriding temperature. The values for AISI 321 steel after removing layers of 5 and 9 μm are also shown.

5. Conclusions

The nitriding experiments and detailed X-ray diffraction, metallographic and compositional analyses in the present work reveal that at low temperatures, a thin, hard and corrosion resistant layer is produced on the investigated austenitic stainless steels by plasma nitriding. An analysis of the X-ray diffraction patterns and their variation with temperature suggests that the low temperature nitrided layers comprise predominantly a single phase, named "S" phase, which has an fcc structure. However, the positions of the diffraction peaks from the "S" phase deviate in a schematic way from those for an ideal fcc lattice. A detailed analysis of the deviation indicates the formation of stacking faults and high compressive residual stresses in the nitrided layer, resulting in a highly distorted and disordered fcc structure. The lattice parameter of the "S" phase was found to increase with increasing nitrogen concentration. The 'S' phase therefore has an fcc crystal structure with a gradually expanded and distorted lattice towards the surface.

Acknowledgement

This work has been funded in part by the European Commission under contract CIPA-CT-94-0151.

References

1. T. BELL and Y. SUN, in Proc. Int. Conf. Surf. Sci. & Eng., edited by Zhu Rhizang, Beijing, May 15–19, 1995 (Int. Academic Publishers, Beijing, 1995) p. 9.
2. B. BILLON and A. HENDRY, *Surf. Eng.* **1**(2) (1985) 114.
3. E. ROLINSKI, *ibid.* **3**(1) (1987) 35.
4. Z. L. ZHANG and T. BELL, *ibid.* **1**(2) (1985) 131.
5. K. ICHII and K. FUJIMURA, edited by E. Broszeit, W. D. Munz, H. Oechsner, K. T. Rie and G. K. Wolf in "Plasma Surface Engineering," Vol. 2 (DGM Informationgesellschaft mbH, Oberursel, 1989) p. 1187.
6. P. A. DEARNLEY, A. NAMVER, G. G. A. HIBBERD and T. BELL, Plasma-Surface Engineering, Vol. 1, p. 219.
7. K. GEMMA, Y. SATOH, I. USHIOKU and M. KAWAKAMI, *Surf. Eng.* **11**(3) (1995) 240.

8. M. SAMANDI, B. A. SHEDDEN, T. BELL, G. A. COLLINS, R. HUTCHINGS and J. TENDYS, *J. Vac. Sci. Technol.* **B12**(2) (1994) 935.
9. E. MENTHE, K-T. RIE, J. W. SCHULTZE and S. SIMSON, *Surf. Coat. Tech.* **74/75** (1995) 412.
10. K. ICHII, K. FUJIMURA and T. TAKASE, *Techn. Rep. Kansai Univ.* **27** (1986) 135.
11. T. ROUX, A. SAKER, C. LEROY, C. FRANTZ and H. MICHEL, in Proc. 9th Int. Congr. Heat. Treat. Surf. Eng., IFHT'94, Nice, France, 1994, p. 291.
12. M. SAMANDI, *Surf. Eng.* **11**(2) (1995) 156.
13. T. BELL and Y. SUN, in "Heat Treatment & Surface Engineering Characterisation & Analytical Methods," Proc. 5th Int. Sem. Heat Treat. Surf. Eng., IFHT, edited by M. Salehi (Isfahan, Eran, 1995) p. 21.
14. E. J. MITTEMEIJER, *J. Metals* **37**(9) (1985) 16.
15. S. R. GOODMAN and HSUN HU, *Trans. Met. Soc. AIME* **230** (1964) 1413.
16. S. V. NAGENDER NAIDU and TRILOK SINGH, *Wear* **166** (1993) 141.
17. C. N. J. WAGNER, J. P. BOISSEAU and E. N. AQUA, *Trans. Met. Soc. AIME* **233** (1965) 1280.
18. C. S. BARRETT, *Trans. AIME, J. Metals* **188** (1950) 123.
19. M. S. PATERSON, *J. Appl. Physics* **23** (1952) 805.
20. B. E. WARREN, *Progr. Metal Phys.* **8** (1959) 147.
21. K. SALMUTTER and F. STANGLER, *Z. Metallk.* **51** (1960) 544.
22. R. E. SCHRAMM and R. P. REED, *Metall. Trans.* **6A** (1975) 1345.
23. X. Y. LI and Y. SUN, unpublished work, 1997.
24. S. P. HANNULA, P. NENONEN and J. MALARIUS, in "High Nitrogen Steels," edited by J. Foct and A. Hendry (The Institute of Metals, London, 1989) p. 266.
25. X. Y. LI, M. Phil Thesis, The University of Birmingham, 1997.

Received 4 December 1997
and accepted 9 March 1999